Water exchange rates and mechanisms in tetrahedral $[Be(H_2O)_4]^{2+}$ and $[Li(H_2O)_4]^{+}$ complexes using DFT methods and cluster-continuum models[i]

Martín Regueiro-Figueroa, David Esteban-Gómez, Rosa Pujales-Paradela, Laura Caneda-Martínez, Andrés de Blas, Carlos Platas-Iglesias[*]

Centro de Investigaciones Científicas Avanzadas (CICA) and Departamento de Química Fundamental, Universidade da Coruña, Campus da Zapateira, Rúa da Fraga 10, A Coruña 15008, Spain

International Journal of Quantum Chemistry, volume 116, issue 19, pages 1388–1396, 5 October 2016
Received 25 April 2016, revised 02 June 2016, accepted 10 June 2016, version of record online 28 June 2016, issue online 18 August 2016

Abstract

The water exchange reactions in aquated Li^{+} and Be^{2+} ions were investigated with density functional theory calculations performed using the $[Li(H_2O)_4]^{+}\cdot 14H_2O$ and $[Be(H_2O)_4]^{2+}\cdot 8H_2O$ systems and a cluster-continuum approach. A range of commonly used functionals predict water exchange rates several orders of magnitude lower than the experimental ones. This effect is attributed to the overstabilization of coordination number four by these functionals with respect to the five-coordinated transition states responsible for the associative (**A**) or associative interchange ($\mathbf{I_a}$) water exchange mechanisms. However, the M06 and M062X functionals provide results in good agreement with the experimental data: M062X/TZVP calculations yield a concerted $\mathbf{I_a}$mechanism for the water exchange in $[Be(H_2O)_4]^{2+}\cdot 8H_2O$ that gives an average residence time of water molecules in the first coordination sphere of 260 μs. For $[Li(H_2O)_4]^{+}\cdot 14H_2O$ the water exchange reaction is predicted to follow an **A** mechanism with a residence time of inner-sphere water molecules of 25 ps.

Keywords: berylium; density functional calculations; lithium; water exchange

Introduction

Exchange reactions involving water molecules in the first and second solvation shells of aquated metal ions are of fundamental importance to understand the reactivity of metal ions in both chemical and biological systems.[1] From the experimental perspective water exchange rate constants are usually determined using NMR techniques, while the pressure dependence of the exchange rate constant provides a valuable tool to assess the water exchange mechanism.[2,3] In an associatively activated water exchange mechanism the

[*] carlos.platas.iglesias@udc.es

entering water molecule approaches the metal ion so that the transition state (TS) is characterized by bond formation, which results in a decrease of volume. On the contrary, a dissociatively activated water exchange mechanism proceeds through a TS characterized by bond breaking, resulting in an increase in volume. Thus, a positive activation volume ($\Delta V^{\ddagger} > 0$) indicates a dissociatively activated water exchange mechanism, while $\Delta V^{\ddagger} < 0$ is indicative of an associatively activated process [$\Delta V^{\ddagger}$ is defined as the difference between the partial volume of the TS and the partial volume of the reactant(s)].[2] However, it is often difficult to decide on the basis of $\Delta V^{\ddagger}$ values whether a given water exchange reaction proceeds through a limiting associative mechanism (**A**) or an associative interchange mechanism ($\mathbf{I_a}$), while the same holds for a limiting dissociative mechanism (**D**) and a dissociative interchange mechanism ($\mathbf{I_d}$).[1-3]

Theoretical methods represent a valuable tool to investigate the mechanism of ligand exchange reactions in metal complexes, providing information on the reaction mechanism at the molecular level.[4] In particular, quantum chemical calculations allow distinguishing among **A**/$\mathbf{I_a}$ or **D**/$\mathbf{I_d}$ mechanisms, as limiting **A** or **D** mechanisms are characterized by stable intermediates on the potential energy surfaces having increased (**A**) or decreased (**D**) coordination numbers. On the contrary, interchange mechanisms are concerted processes.[5] Furthermore, theoretical calculations provide direct information on ligand exchange reactions of labile complexes that are too fast to be observed on the NMR time scale. For instance, Merbach and co.[6] applied variable-pressure NMR techniques to investigate the water exchange mechanism in $[Be(H_2O)_4]^{2+}$, reporting an activation volume of $\Delta V^{\ddagger} = -13.6$ cm^3 mol^{-1}. The latter value is close to the extreme value predicted for an **A** mechanism in octahedral complexes (−13 cm^3 mol^{-1}),[7] and thus an associative mechanism was suggested. However, a $\mathbf{I_a}$ mechanism was proposed later by van Eldik on the basis of density functional theory (DFT) calculations performed in the gas-phase (B3LYP/6-311 + G**).[8] In a similar study, the same group proposed an **A** mechanism for $[Li(H_2O)_4]^+$,[9] a system presenting a very fast water exchange rate that is difficult to determine experimentally.

DFT methods represent a very attractive approach for the investigation of ligand exchange reactions in metal complexes due to its relatively good accuracy and favorable scaling with system size.[10] However, different studies have pointed out some limitations of DFT methods in this context.[11] For instance, early DFT studies performed on $[M(H_2O)_6]^{3+}\cdot H_2O$ systems (M = Ti, V) resulted in a proton transfer from a coordinated water molecule to the second sphere water molecule, providing a $[M(H_2O)_5(OH)\cdot H_3O]^{3+}$ species.[12,13] However, this problem might be overcome by including an explicit second-hydration shell, which allows calculating hydrolysis constants of divalent and trivalent metal ions to an accuracy of 1–2 pH units.[14] Furthermore, the explicit inclusion of a second-hydration shell, often in combination with the inclusion of polarized continuum solvation models, allows an accurate calculation of vibrational spectra[15-20] and ^{1}H and ^{17}O hyperfine coupling constants of coordinated water molecules.[21] Another limitation of DFT is its known trend to stabilize low coordination numbers (10–55 kJ mol^{-1} for B3LYP), which favors **D**/$\mathbf{I_d}$ mechanisms over associative (**A**/$\mathbf{I_a}$) ones.[22,23]

In this work, we present a DFT study on the structure and water exchange mechanism of the $[Li(H_2O)_4]^+$ and $[Be(H_2O)_4]^{2+}$ aqua ions, which are the only metal ions presenting tetrahedral structures in solution. The low coordination numbers reduce the computational cost of the calculations, which facilitates testing different computational recipes that could be subsequently extended to aqua ions with higher coordination numbers. In the case of $[Be(H_2O)_4]^{2+}$, the water exchange reaction could be studied experimentally using NMR techniques, which furnishes a complete set of experimental data to assess the accuracy of the calculations. For this purpose, we performed calculations using a mixed cluster/continuum approach that includes an explicit second solvation shell. Such mixed cluster/continuum approaches were found to perform better than pure continuum models to describe ionic solutes with high charge densities.[24,25] We will show that an adequate selection of the functional is critical to obtain results in good agreement with the experimental values.

Computational methods

Full geometry optimizations of the $[Be(H_2O)_4]^{2+}\cdot 8H_2O$, $[Li(H_2O)_4]^{+}\cdot 8H_2O$, and $[Li(H_2O)_6]^{+}\cdot 12H_2O$ systems were performed in aqueous solution employing DFT with the GGA functionals PBE[26,27] and BLYP[28,29] and their hybrid analogues PBE0[30] and B3LYP[31] functionals, the meta-GGA M06L[32] and TPSS[33] functionals, the hybrid meta-GGA TPSSh,[33] M062X,[32] and M06[32] functionals and the long range corrected version of B3LYP CAM-B3LYP.[34] Bulk solvent effects (water) were considered by using the integral equation formalism variant of the polarizable continuum model.[35] In PCMs, the solute cavity is constructed by a set of interlocking spheres centered on the solute atoms or atomic groups. The universal force field radii (UFF)[36] scaled by a factor of 1.1 were used for Li^+ (1.2255 Å) and Be^{2+} (1.3725 Å).[37] Geometry optimizations using the UFF radii scaled by 1.1 for O (1.750 Å) and H (1.443 Å) often failed, providing an error on the total polarization charges (value of the density outside the generated cavity) that exceeded 0.05 a. u.[38] Thus, we used larger radii for O and H (1.925 and 1.587 Å, respectively) to ensure an error on total polarization charges well below the 0.05 a. u. threshold and facilitate the convergence of geometry optimizations. Most of the calculations were performed using the standard Ahlrichs' valence triple-ξ basis set including polarization functions (TZVP).[39] Other basis sets tested in this work included the SVP basis set of Ahlrichs,[40] the basis sets of the Pople's family 6-31G and 6-311G supplemented with diverse sets of polarization and diffuse functions,[41-46] and Dunning's correlation consistent basis sets cc-pVXZ (X = D or T) and aug-cc-pVXZ (X = D, T, Q and 5).[47] No symmetry constraints have been imposed during the optimizations. The stationary points found on the potential energy surfaces were characterized by using frequency analysis. The nature of the saddle points (one imaginary frequency) was also characterized by frequency analysis. Frequency calculations provided zero-point energies (ZPEs), enthalpies (*H*), and free energies (*G*) at 298.15 K and 1 atm. The relative free energies of energy minima and TSs include nonpotential-energy contributions (ZPEs and thermal terms) obtained through frequency analysis. A superfine integration grid (150 radial shells and 974 angular points) was used throughout, while the SCF energy convergence criterion was set to 10^{-8} a. u. Molecular volumes, defined as the volume inside a contour of the electron density of 0.001 e $bohr^{-3}$, were calculated using the volume = tight keyword in Gaussian 09. All calculations were performed using the Gaussian 09 package (Revision D.01).[48] Molecular graphics were generated using USCF Chimera (version 1.8).[49]

Results and discussions

Optimized geometries of the $[Be(H_2O)_4]^{2+}\cdot 8H_2O$ and $[Li(H_2O)_4]^{+}\cdot 8H_2O$ systems

In a series of papers Pye et al.[50-54] reported vibrational (IR and Raman) and computational (MP2 and B3LYP) studies on the hydration of Li^+ and Be^{2+} in aqueous solutions. These investigations demonstrated that both cations are four-coordinated in diluted aqueous solutions. In the case of Li^+ there has been some debate about the number of water molecules coordinated to the metal ion in solution,[55] but the theoretical community reached consensus that four water molecules preferentially coordinate Li^+ in diluted aqueous solutions under standard conditions.[56,57] Recent neutron scattering studies provided a hydration number of ~4.8(3), which was found to be independent of ion concentration.[58] In the solid state, the structures of aquated Li^+ generally present coordination number four, although some structures with coordination numbers five[59,60] and even six[61] have been reported. However, aquated Be^{2+} ions present systematically tetrahedral coordination in the solid state.[62-67]

Geometry optimizations of the $[Be(H_2O)_4]^{2+}\cdot 8H_2O$ system were carried out using different density functionals (Table 1). All optimized geometries present nearly undistorted S_4symmetries very similar to those reported by Pye (Figure 1).[53,54] Four water molecules are coordinated to the Be^{2+} ion providing a fairly regular tetrahedral coordination environment. The eight second-sphere water molecules establish a

hydrogen-bonding network so that each coordinated water molecule acts as a hydrogen-bond donor to two second-sphere water molecules. Pairs of second-sphere water molecules are also joined by hydrogen bonds. The calculated Be–O bond distances and O–Be–O angles are in good agreement with those determined in the solid state using X-diffraction measurements. Indeed, a search in the Cambridge Structural Database (CSD version 5.36, 2015 release) provides seven entries containing $[Be(H_2O)_4]^{2+}$ entities that show tetrahedral coordination geometries with Be–O distances in the range 1.593–1.636 Å.[62-67] The O–Be–O bond angles determined in the solid state present relatively small deviations from the ideal tetrahedral angle, falling in the range 104.9–117.9°. The calculated Be–O distances agree also quite well with the value determined in solution using neutron diffraction experiments.[68] Overall, the data reported in Table 1 show that all functionals explored in this work provide very similar geometries. Furthermore, all functionals provide very similar vibrational frequencies of the BeO_4skeleton, which in turn are in good agreement with the experimental values (Table 1).[53]

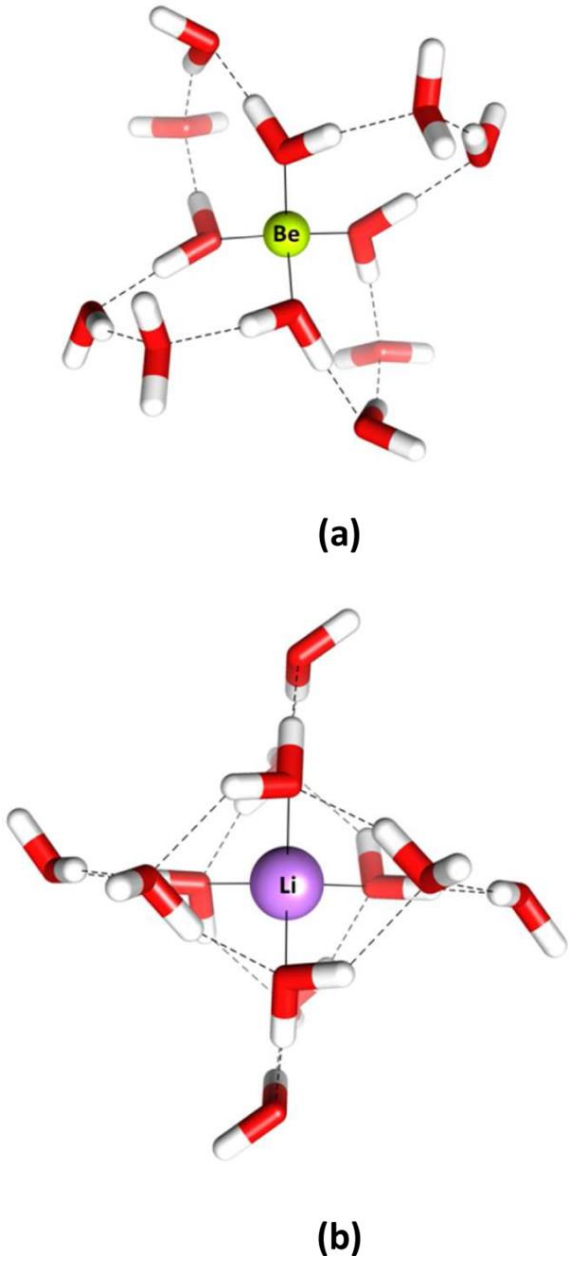

Figure 1. Geometries of the $[Be(H_2O)_4]^{2+}\cdot 8H_2O$ (a, S_4#1) and $[Li(H_2O)_4]^{+}\cdot 8H_2O$ (b, S_4#2) systems optimized in aqueous solution at the M062X/TZVP level

Table 1. Calculated bond distances (Å) and angles (º) of the metal coordination environment and harmonic frequencies (cm^{-1}) of the BeO_4 skeletal modes of $[Be(H_2O)_4]^{2+}\cdot 8H_2O$[a]

	Be–O	**O–Be–O**	ν_1	ν_2	ν_3	ν_4
BLYP	1.654	108.0	500	267	714	326
		110.2			731	
B3LYP	1.637	108.5	520	273	744	336
		110.0			753	
CAM-B3LYP	1.627	108.8	532	279	766	344
		109.8				
PBE	1.646	107.8	512	270	757	334
		110.3				
PBE0	1.630	108.4	528	275	767	344
		110.0				
TPSS	1.643	107.9	514	278	748	336
		110.3				
TPSSh	1.637	108.1	518	277	769	346
		110.2				
M06L	1.629	108.5	524	277	773	344
		109.9				
M06	1.627	105.4	513	264	739	340
		111.6	750			
M062X	1.621	108.4	542	274	776	332
		110.0				
Exp.	1.60[b]		531[c]	–	760[c]	348[c]

[a] All calculations employed the TZVP basis set. [b] Neutron diffraction measurements in solution from reference 68. [c] IR and Raman data from reference 53.

Table 2. Calculated bond distances and angles of the metal coordination environment and harmonic frequencies of the LiO_4 skeletal modes of $[Li(H_2O)_4]^{+}\cdot 8H_2O$[a]

	Li–O (Å)	**O–Li–O (º)**	**Li···H (Å)**	ν_1 **(cm^{-1})**
PBE0	2.042	94.4	2.468	217
		117.5	2.578	
TPSS	2.046	84.2	2.475	167
		117.6	2.579	
TPSSh	2.034	94.5	2.465	208
		117.5	2.570	
M062X	1.962	96.1	2.429	319
		116.5	2.512	
Exp.	1.94–1.97[b]		2.56–2.58	250[c]

[a] All calculations employed the TZVP basis set. [b] Neutron scattering measurements in solution from reference 58. [c] IR and Raman data from reference 51.

Geometry optimizations of the $[Li(H_2O)_4]^+ \cdot 8H_2O$ system provide two minimum energy structures with S_4 symmetry, one analogous to that obtained for Be^{2+} (denoted as S_4#1) and a second one in which the coordinated water molecules act as hydrogen-bond acceptors, establishing an additional hydrogen bond with a second-sphere water molecule (denoted as S_4#2). This provides an additional stabilization to the $[Li(H_2O)_4]^+ \cdot 8H_2O$ cluster, as the S_4#2 form presents a relative Gibbs free energy of −15.6 kJ mol^{-1} with respect to the S_4#1 one (at the M062X/TZVP level). In the case of $[Be(H_2O)_4]^{2+} \cdot 8H_2O$, the S_4#2 structure is not stable, which is likely related to the higher positive charge of the central ion. Indeed, the S_4#2 structure in $[Li(H_2O)_4]^+ \cdot 8H_2O$ presents a set of four second-sphere water molecules with one of the hydrogen atoms pointing to the coordinated water molecules with Li···H distances of only 2.733 Å (at the M062X/TZVP level). The Li–O bond distances of the S_4#2 structure of $[Li(H_2O)_4]^+ \cdot 8H_2O$ calculated using the PBE0, TPSS, and TPSSh functionals are somewhat longer than those observed in aqueous solution using neutron scattering studies, while the Li–O distance obtained at the M062X/TZVP level (1.962 Å) is in excellent agreement with the experiment (Table 2). However, the frequencies of the symmetric LiO_4 stretching mode calculated with the different functionals present significant deviations from the experimental value (Table 2). In contrast to the Be^{2+} case, the calculated structures of the $[Li(H_2O)_4]^+ \cdot 8H_2O$ system present relatively large deviations of the calculated O–Li–O angles from the ideal value expected for a tetrahedral coordination.

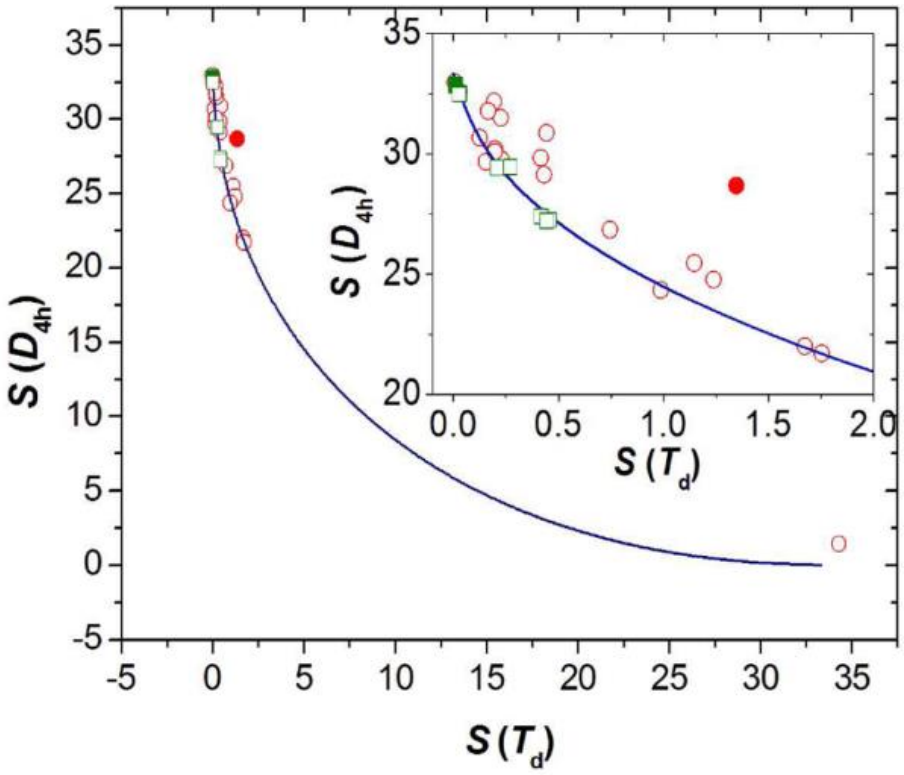

Figure 2. Symmetry map obtained for tetracoordinated $[Li(H_2O)_4]^+$ (red open circles) and $[Be(H_2O)_4]^{2+}$ (green open squares) complexes observed in X-ray crystal structures. S(D_{4h}) and S(T_d) represent the symmetry measures for square planar and tetrahedral coordination. The solid line represents the minimum distortion path that connects the tetrahedron and the square. Filled symbols correspond to the data obtained for the $[Be(H_2O)_4]^{2+} \cdot 8H_2O$ and $[Li(H_2O)_4]^+ \cdot 8H_2O$ systems at the M062X/TZVP level

A search in the CSD provides 20 examples of discrete $[Li(H_2O)_4]^+$ complexes with tetrahedral geometries having varying degrees of distortion, and one structure showing square planar coordination.[69] The Li–O bond distances and O–Li–O angles observed in the tetrahedral structures vary considerably, with values ranging from 1.824 to 2.036 Å (distances) and 94.4 to 129.3º (angles). The coordination polyhedra of

$[Li(H_2O)_4]^+$ and $[Be(H_2O)_4]^{2+}$ complexes determined by X-ray diffraction measurements were analyzed quantitatively by performing shape measures.[70] The shape measure, S(A), is zero for a structure fully coincident in shape with the reference polyhedron and the maximum allowed value of S(A) is 100.[71] The analysis of the crystallographic data of $[Be(H_2O)_4]^{2+}$ provides shape measures for tetrahedral coordination in the range 0.02–0.46, reflecting rather small distortions from the ideal tetrahedral geometry (Figure 2). In the case of $[Li(H_2O)_4]^+$ the S(A) values (S(A) = 0.01 – 1.75) present more important deviations from the ideal tetrahedral geometry, and noteworthy one of the structures displays a S(A) value of 34.3 for a tetrahedral polyhedron and 1.43 for a square planar coordination.[69] Interestingly, the shape measures obtained for both complexes follow rather well the minimum distortion path that connects the tetrahedron and the square (Figure 2).

The structures calculated for $[Be(H_2O)_4]^{2+}\cdot 8H_2O$ and $[Li(H_2O)_4]^+\cdot 8H_2O$ present S(A) values also falling close to the minimum distortion path and similar to those obtained experimentally (Figure 2). Taken together, these results point to a rather flat potential energy surface of the $[Li(H_2O)_4]^+$ complex, while for $[Be(H_2O)_4]^{2+}$ the tetrahedral geometry appears to define a rather deeper minimum in the potential energy surface.

Water exchange in $[Be(H_2O)_4]^{2+}\cdot 8H_2O$

The water exchange reaction in $[Be(H_2O)_4]^{2+}\cdot 8H_2O$ was investigated by using DFT calculations. A range of representative functionals were employed in these calculations in combination with the TZVP basis set. Approaching a second-sphere water molecule to the central Be^{2+} ion results in a five-coordinate TS with trigonal bipyramidal coordination around the metal ion (Figure 3). Whatever the density functional employed the entering (O1) and leaving (O2) water molecules occupy the axial positions of the coordination polyhedron, with Be–O distances somewhat longer than those involving the three equatorial water ligands (Figure 3, see also Table 3). These results point to an associative interchange (**I_a**) water exchange mechanism instead of an associatively activated mechanism, which should proceed with the formation of a stable five-coordinate intermediate species. A similar conclusion was reached by van Eldik et al. on the basis of B3LYP/6-311 + G** calculations performed on the $[Be(H_2O)_4]^{2+}\cdot H_2O$ system.[8] However, while all functionals tested in this work provided an **I_a** mechanism, the calculated activation parameters were found to vary dramatically depending on the DFT model. The BLYP, B3LYP, CAM-B3LYP, PBE, PBE0, TPSS, and TPSSh functionals provide relatively similar activation parameters (Table 3), with activation enthalpies $\Delta H^{\ddagger}$ in the range 54.4–62.8 kJ mol^{-1} and activation entropies of $\Delta S^{\ddagger} = -47.5$ to -62.5 J mol^{-1} K^{-1}. The negative activation entropy is expected for an associatively activated water exchange mechanism, and is in line with the experimental value reported by Füldner (-44 J mol^{-1} K^{-1}).[72] A slightly positive $\Delta S^{\ddagger}$ value was determined by Merbach et al.,[6] although the water exchange rates determined by these two groups are in reasonably good mutual agreement. However, these functionals provide activation free energies that exceed by far the experimental values, which results in rate constants k_{ex}^{298} 2–4 orders of magnitude smaller than the experimental values (Table 3). Furthermore, the calculated activation volumes range from clearly positive (+9.7 cm^3 mol^{-1} at the B3LYP/TZVP level) to clearly negative (-16.2 cm^3 mol^{-1} at the TPSSh/TZVP level).

The results obtained using the M06 and M062X functionals provide an important improvement in terms of the agreement with experimental data (Table 3). These functionals were developed by Truhlar using a wide range of databases that included thermochemical data. The calculated activation free energies at 298.15 K ($\Delta G_{298}^{\ddagger} = 53.6$ and 52.7 kJ mol^{-1} using M06 and M062X, respectively) are in excellent agreement with the experiment, while the $\Delta H^{\ddagger}$and $\Delta S^{\ddagger}$ values are close to those reported by Füldner.[72] Furthermore, the calculated $\Delta V^{\ddagger}$values present also an excellent agreement with that determined by Merbach using variable pressure NMR measurements. These results are in line with previous findings that showed that the M06 functional is competitive with high level *ab initio* methods for investigating water exchange reactions in actinyl complexes.[73] The data collected in Table 3 indicate that the relative electronic energies of the

reactant and TS ($\Delta E^{\ddagger}$) are the main responsible for the different activation parameters obtained with M06 and M062X with respect to the other functionals investigated in this work, while zero point energy corrections and thermal corrections to enthalpy play a minor role.

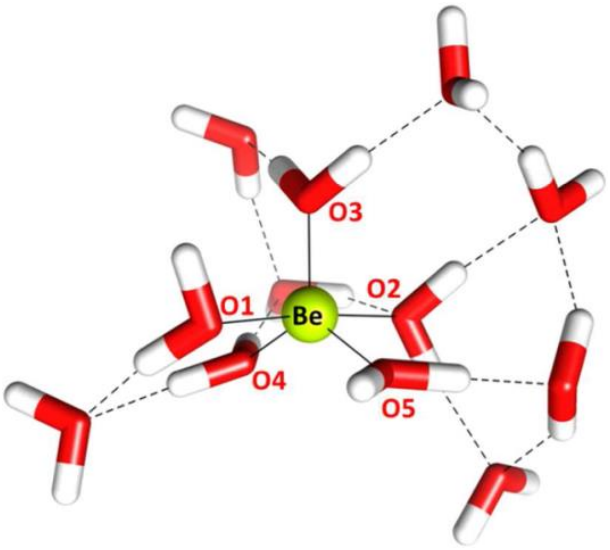

Figure 3. Transition state (TS) calculated at the M062X/TZVP level for the water exchange reaction in $[Be(H_2O)_4]^{2+}\cdot 8H_2O$. Bond distances of the metal coordination environment (Å): Be-O1, 2.001; Be-O2, 2.049; Be-O3, 1.615; Be-O4, 1.622; Be-O5, 1.630. Bond angles (º): O1-Be-O2, 175.2; O1-Be-O3, 92.5; O1-Be-O4, 91.6; O1-Be-O5, 86.9; O2-Be-O3, 92.2; O2-Be-O4, 86.9; O2-Be-O5, 90.2; O3-Be-O4, 116.6; O3-Be-O5, 119.1; O4-Be-O5, 124.3

The exchange rates of the water exchange reactions (k_{ex}) and residence times of the coordinated water molecules (τ) were estimated using TS theory with the following expressions:[74,75]

$$k_{\mathrm{ex}} = \frac{1}{\tau} = \Gamma_n \kappa \frac{k_{\mathrm{B}}\mathrm{T}}{\mathrm{h}} e^{-\Delta G^{\neq}/RT} \qquad (1)$$

$$\Gamma_n = 1 + \frac{1}{24}\left(\frac{h\nu^{\neq}}{k_{\mathrm{B}}T}\right)^2 \qquad (2)$$

Where k_B is the Boltzman constant, h the Planck's constant, R the gas constant, $\Delta G^{\ddagger}$represents the free energy difference between the intermediate and the TS (at 298.15 K), κ is the transition probability assumed to be 1, Γ_n is the tunneling factor, and $\nu^{\ddagger}$ is the imaginary frequency characterizing the TS. The imaginary frequencies obtained using different functionals are in the range 237i–280i, which provide tunneling factors of 1.054–1.076. The exchange rates given in Table 3 clearly show that among the functionals investigated in this work only M06 and M062X provide the right order of magnitude of $k_{ex.}$

The water exchange reaction in $[Be(H_2O)_4]^{2+}\cdot 8H_2O$ was also investigated using the M06 functional and a number of basis sets ranging from split valence to triple-ξ quality including different sets of polarization and diffuse functions. Geometry optimizations of $[Be(H_2O)_4]^{2+}\cdot 8H_2O$ using some basis sets (SVP, 6-31G(d,p)) suffered from convergence problems or converged to geometries having one or two imaginary frequencies.

Table 3. Bond distances of the metal coordination environment, activation parameters and rate constants obtained from the TSs associated to the water exchange reaction in $[Be(H_2O)_4]^{2+}\cdot 8H_2O$ (basis set: TZVP)

	Be–O (TS)/Å	$\Delta H^{\ddagger}$	$\Delta E^{\ddagger}_{ZPE}$	$\Delta H^{\ddagger a}$	$\Delta S^{\ddagger b}$	$\Delta G^{\ddagger a}$	$\Delta V^{\ddagger c}$	k_{ex}^{298} (s^{-1})
B3LYP	2.141/2.151	63.0	65.6	61.7	−62.5	80.4	+9.7	0.05
	1.610/1.614/1.626							
BLYP	2.211/2.217	64.6	65.8	62.8	−47.5	77.0	+2.1	0.21
	1.617/1.621/1.635							
CAM-B3LYP	2.091/2.099	55.5	59.2	55.2	−58.7	72.8	−8.2	1.21
	1.608/1.613/1.623							
PBE	2.122/2.138	56.1	57.9	54.4	−51.3	69.7	−0.9	4.08
	1.621/1.632/1.644							
PBE0	2.075/2.086	58.4	60.5	57.3	−49.9	72.1	+2.5	1.58
	1.614/1.622/1.631							
TPSS	2.075/2.078	60.7	62.2	59.1	−49.9	74.0	−7.3	0.72
	1.629/1.641/1.649							
TPSSh	2.056/2.072	61.3	63.0	60.0	−48.0	74.3	−16.2	0.62
	1.625/1.636/1.643							
M06	2.084/2.124	36.6	39.4	35.5	−60.7	53.6	−12.4	2716
	1.612/1.613/1.623							
M062X	2.001/2.049	33.4	37.9	33.8	−63.6	52.7	−14.1	3848
	1.615/1.622/1.630							
Exp.6, 72				41.5	−44	54.6		1800
				59.2	+8.4	56.7	−13.6	730

[a] Values in kJ mol^{-1}; Activation free energies are calculated at 298.15 K. [b] Values in J mol^{-1} K^{-1}. [c] Values in cm^3 mol^{-1}.

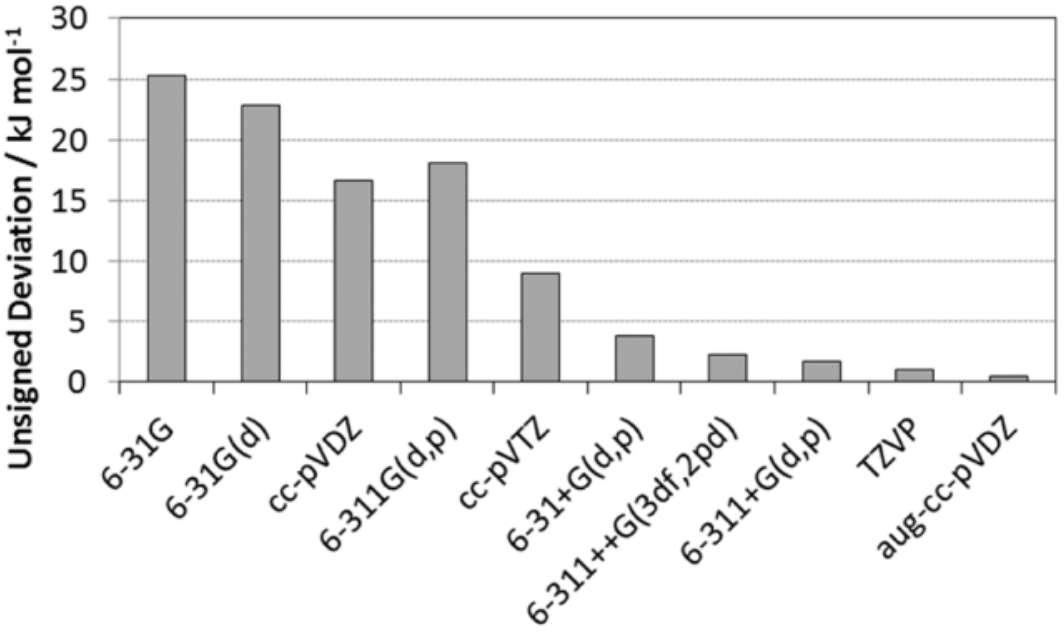

Figure 4. Unsigned deviations of the calculated activation free energies ($\Delta G^{\ddagger}$) obtained with the M06 functional and different basis sets for the water exchange reaction in $[Be(H_2O)_4]^{2+}\cdot 8H_2O$

The unsigned deviations between the calculated and experimental activation free energies $\Delta G^{\ddagger}$ (Figure 4, see also Table S1, Supporting Information) show that the split valence basis sets 6-31G and 6-31G(d), the double-ξ cc-pVDZ basis set and even the triple-ξ 6-311G(d,p) basis set provide very large deviations from the experimental data (16.6 to 25.3 kJ mol^{-1}). Even the polarized triple-ξ cc-pVTZ basis set gives a rather large deviation, while a dramatic improvement is observed on inclusion of diffuse functions. Thus, the 6-31 + G(d,p), 6-311 + G(d,p), 6-311++G(3df,2pd), and aug-cc-pVDZ basis sets give results in very good agreement with the experiment. These results highlight the importance of including diffuse functions to improve the quality of the calculated reaction barrier heights with DFT, as pointed out by Truhlar.[76] The TZVP basis set also provides excellent results.

Water exchange in $[Li(H_2O)_4]^+ \cdot 14H_2O$

The water exchange reaction in $[Li(H_2O)_4]^+$ was first investigated using the $[Li(H_2O)_4]^+ \cdot 8H_2O$ system described above. Calculations performed at the M062X/TZVP level revealed a five-coordinate intermediate with square pyramidal (SP) coordination around the metal ion. However, since some X-ray structures presented six-coordinated $[Li(H_2O)_6]^+$ species in the solid state,[61] we decided to use a $[Li(H_2O)_6]^+ \cdot 12H_2O$ model to investigate the relative stabilities of the six-, five-, and four-coordinated forms of aquated Li^+. Indeed, the inclusion of two second-sphere water molecules for each coordinated water molecule was found to provide an adequate description of the second coordination shell in different octahedral aqua complexes.[15-18,20,21] The optimized geometry of $[Li(H_2O)_6]^+ \cdot 12H_2O$ presents a S_6symmetry with an arrangement of the second-sphere water molecules very similar to those reported for different octahedral aqua ions.[19] The $[Li(H_2O)_6]^+ \cdot 12H_2O$ structure optimized at the M062X/TZVP level presents Li–O distances of 2.15 Å and a hydrogen-bonding pattern of the second-sphere water molecules similar to that described above for $[Li(H_2O)_4]^+ \cdot 8H_2O$ (Supporting Information). Increasing one of the Li–O distances leads to a five-coordinated $[Li(H_2O)_5]^+ \cdot 13H_2O$ species showing a SP coordination environment with Li–O distances involving water molecules of the basal plane in the range 2.04–2.16 Å and a $Li–O_{apical}$distance of 2.00 Å (Figure 5). A careful analysis of the potential energy surface reveals the presence of two virtually isoenergetic energy minima with tetrahedral coordination geometry around the Li^+ ion [T_d(1) and T_d(2)] that are connected to the square-pyramidal intermediate by TSs TS1 and TS2 (Figure 6). The relative electronic energy of the SP intermediate with respect to the T_d structures is rather small ($\Delta E = 2.63$ kJ mol^{-1}), while the inclusion of zero-point-energy corrections increases this value to $\Delta E_{ZPE} = 4.66$ kJ mol^{-1}. The relative free energy amounts to 7.29 kJ mol^{-1}. On the contrary, the octahedral $[Li(H_2O)_6]^+ \cdot 12H_2O$ structure presents a very high relative energy with respect to the tetrahedral forms ($\Delta E_{ZPE} = 31.1$ kJ mol^{-1} and $\Delta G = 24.4$ kJ mol^{-1}), and therefore, we conclude that octahedral structures do not play a significant role in the water exchange reactions of aquated Li^+.

The potential energy surface calculated at the M062X/TZVP level is characteristic of an associative exchange process (**A** mechanism) that proceeds with the formation of a five-coordinated intermediate. According to our calculations, the energy of TS1 is higher than that of TS2, and therefore the rate determining step for the exchange reaction corresponds to the approach of the entering water molecule to form the square-pyramidal intermediate, rather than the departure of the leaving water molecule. The activation free energy for the exchange reaction, as calculated from the energy of TS1 amounts to $\Delta G^{\ddagger}_{298} = 12.5$ kJ mol^{-1}, with $\Delta H^{\ddagger} = 6.6$ kJ mol^{-1}, and $\Delta S^{\ddagger} = -20.0$ J mol^{-1} K^{-1}. The negative activation entropy is in line with an **A** water exchange mechanism. The calculated activation volume is negative ($\Delta V^{\ddagger} = -5.2$ cm^3 mol^{-1}). The activation free energy obtained from these calculations corresponds to a water exchange rate at 25°C of $k_{ex}^{298} = 3.9 \times 10^9$ s^{-1} and an average residence time of water molecules in the first coordination sphere of 25 ps (Γ_n =1.007, $\nu^{\ddagger}$ =84i). This value is in excellent agreement with the experimental estimate obtained with quasi-elastic neutron scattering studies (< 100 ps)[77] and different molecular dynamics studies, which provided mean residence times in the range 25–400 ps.[78]

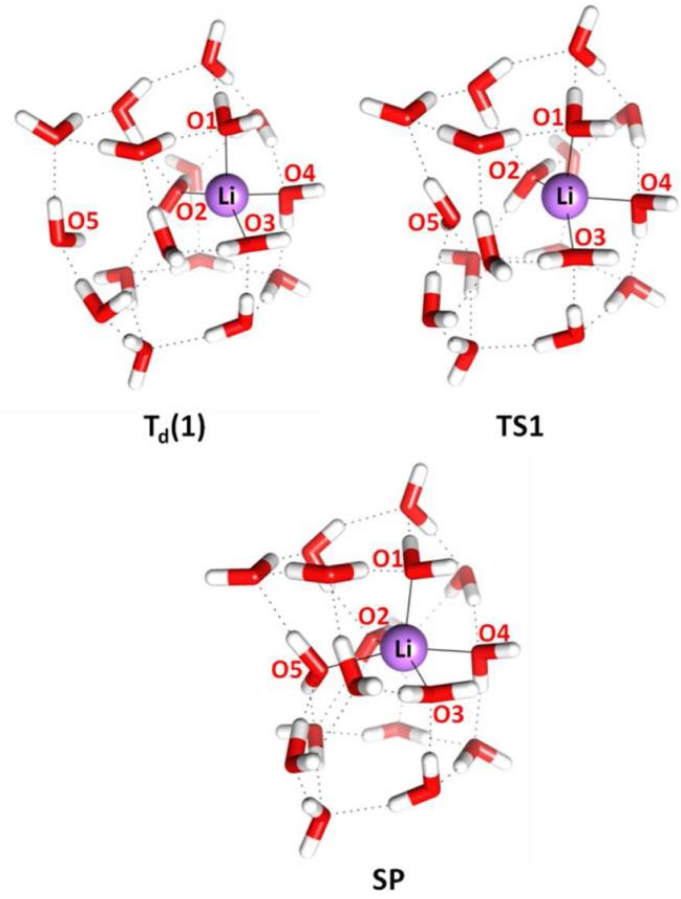

Figure 5. Geometries of the energy minimum ($T_d(1)$), TS (TS1), and intermediate (SP) involved in the water exchange reaction of $[Li(H_2O)_4]^+ \cdot 14H_2O$ as optimized in aqueous solution at the M062X/TZVP level

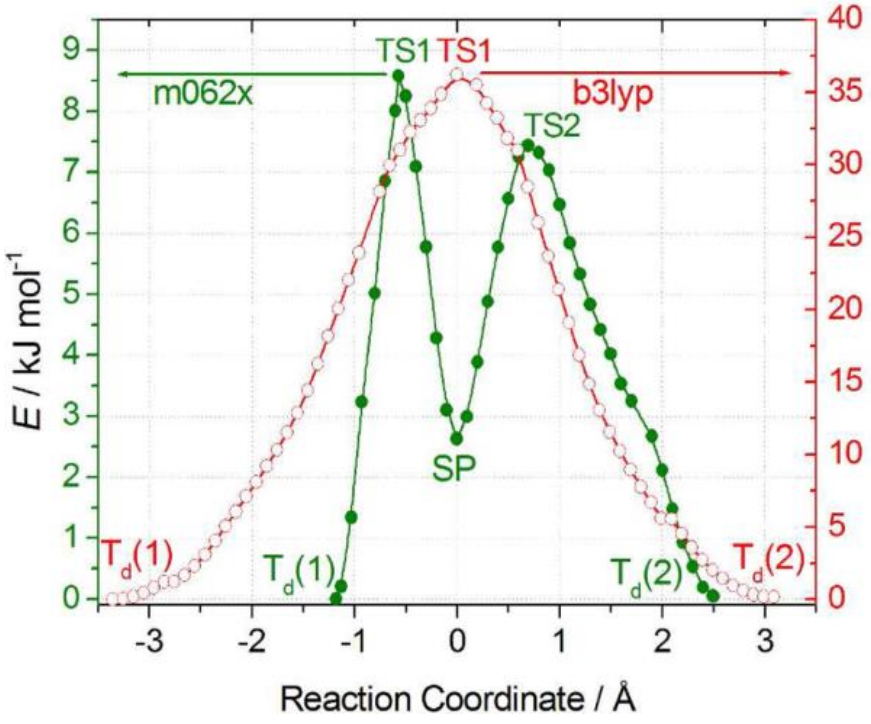

Figure 6. Relaxed potential energy surfaces generated for the $[Li(H_2O)_4]^+ \cdot 14H_2O$ at the M062X/TZVP and B3LYP/TZVP levels. Negative values of the reaction coordinate correspond to the approach of the entering water molecule (O5) while positive values represent the lengthening of the Li-O4 distance

The water exchange reaction in $[Li(H_2O)_4]^+ \cdot 14H_2O$ was also investigated at the B3LYP/TZVP level for comparative purposes. The relaxed potential energy surface calculated at this level is presented in Figure 6. In contrast to the M062X results, at the B3LYP/TZVP level the water exchange reaction proceeds through a concerted (**I_a**) mechanism. All attempts to locate a five-coordinate intermediate failed. Furthermore, the energy of the TS connecting the $T_d(1)$ and $T_d(2)$ energy minima is ~4 times higher than that calculated at the M062X/TZVP level. The activation parameters obtained at the B3LYP level ($\Delta G^{\ddagger}_{298} = 43.7$ kJ mol^{-1}, with $\Delta H^{\ddagger} = 36.5$ kJ mol^{-1}, and $\Delta S^{\ddagger} = -24.15$ J mol^{-1} K^{-1}) yield a water exchange rate at 25°C of $k_{ex}^{298} = 1.39 \times 10^5$ s^{-1}and an average residence time of inner-sphere water molecules of 7.2 μs (Γ_n =1.012, $\nu^{\ddagger}$=111i). Thus, B3LYP overestimates the residence time of coordinated water molecules by five orders of magnitude compared to both the M062X results and the experimental data.

Conclusions

In summary, we have shown that water exchange mechanisms and activation parameters in tetrahedral $[Li(H_2O)_4]^+$ and $[Be(H_2O)_4]^{2+}$ can be calculated to a good accuracy using cluster-continuum models. In these calculations, an adequate selection of the density functional is of critical importance. Among the functionals explored in this work only the M06 and M062X functionals provided results in good agreement with the available experimental data, while functionals such as B3LYP overstabilize low coordination numbers and therefore disfavor **A**and **I_a** mechanisms. Thus, the M06 and M062X functionals are recommended to investigate ligand exchange reactions in Li^+ and Be^{2+} complexes.

Funding Information

Ministerio de Economía y Competitividad (CTQ2013-43243-P and CTQ2015-71211-REDT) for generous financial support.

Acknowledgements

The authors are also indebted to Centro de Supercomputación de Galicia (CESGA) for providing the computer facilities.

References

[1] L. Helm, A. E. Merbach, *Chem. Rev.* **2005**, *105*, 1923.

[2] C. D. Hubbard, R. Van Eldik, *Inorg. Chim. Acta* **2010**, *363*, 2357.

[3] F. A. Dunand, L. Helm, A. E. Merbach, *Adv. Inorg. Chem.* **2003**, *54*, 1.

[4] H. Erras-Hanauer, T. Clark, R. Van Eldik, *Coord. Chem. Rev.* **2003**, *238–239*, 233.

[5] C. H. Langford, H. B. Gray, *Ligand Substitution Processes*, W. A. Benjamin, Inc., New York **1966**.

[6] P.-A. Pittet, G. Elbaze, L. Helm, A. E. Merbach, *Inorg. Chem.* **1990**, *29*, 1936.

[7] T. W. A. Swaddle, *Inorg. Chem.* **1983**, *22*, 2663.

[8] R. Puchta, N. Van Eikema Hommes, R. Van Eldik, *Helv. Chim. Acta* **2005**, *88*, 911.

[9] R. Puchta, M. Galle, N. Van Eikema Hommes, E. Pasgreta, R. Van Eldik, *Inorg. Chem.* **2004**, *43*, 8227.

[10] T. Ziegler, *J. Chem. Soc. Dalton Trans.* **2002**, 642.

[11] F. P. Rotzinger, *Chem. Rev.* **2005**, *105*, 2003.

[12] M. Hartmann, T. Clark, R. Van Eldik, *J. Phys. Chem. A* **1999**, *103*, 9899.

[13] M. Benmelouka, S. Messaoudi, E. Furet, R. Gautier, E. Le Fur, J.-Y. Pivan, *J. Phys. Chem. A* **2003**, *107*, 4122.

[14] M. C. F. Wander, J. R. Rustad, W. H. Casey, *J. Phys. Chem. A* **2010**, *114*, 1917.

[15] G. D. Markham, J. P. Glusker, C. W. Bock, *J. Phys. Chem. B* **2002**, *106*, 5118.

[16] W. W. Rudolph, C. C. Pye, *J. Phys. Chem. A* **2000**, *104*, 1627.

[17] J. Li, C. L. Fisher, J. L. Chen, D. Bashford, L. Noodleman, *Inorg. Chem.* **1996**, *35*, 4694.

[18] C. C. Pye, W. W. Rudolph, *J. Phys. Chem. A* **1998**, *102*, 9933.

[19] C. W. Bock, G. D. Markham, A. K. Katz, J. P. Glusker, *Theor. Chem. Acc.* **2006**, *115*, 100.

[20] M. Pavlov, P. E. M. Siegbahn, M. Sandström, *J. Phys. Chem. A* **1998**, *102*, 219.

[21] D. Esteban-Gómez, C. Cassino, M. Botta, C. Platas-Iglesias, *RSC Adv.* **2014**, *4*, 7094.

[22] F. P. Rotzinger, *J. Phys. Chem. B* **2005**, *109*, 1510.

[23] P. Wahlin, C. Danilo, V. Vallet, F. Real, J.-P. Flament, U. Wahlgren, *J. Chem. Theory Comput.* **2008**, *4*, 569.

[24] V. S. Bryantsev, M. S. Diallo, W. A. Goddard, III, *J. Phys. Chem. A* **2009**, *113*, 9559.

[25] Z. Qian, H. Feng, W. Yang, Q. Miao, L. He, S. Bi, *Chem. Commun.* **2008**, 3930.

[26] J. P. Perdew, K. Burke, M. Ernzerhof, *Phys. Rev. Lett.* **1996**, *77*, 3865.

[27] J. P. Perdew, K. Burke, M. Ernzerhof, *Phys. Rev. Lett.* **1997**, *78*, 1396.

[28] A. D. Becke, *Phys. Rev. A* **1988**, *38*, 3098.

[29] C. Lee, W. Yang, R. G. Parr, *Phys. Rev. B* **1988**, *37*, 785.

[30] C. Adamo, V. Barone, *J. Chem. Phys.* **1999**, *110*, 6158.

[31] A. D. Becke, *J. Chem. Phys.* **1993**, *98*, 5648.

[32] Y. Zhao, D. G. Truhlar, *Theor. Chem. Acc.* **2008**, *120*, 215.

[33] J. Tao, J. P. Perdew, V. N. Staroverov, G. E. Scuseria, *Phys. Rev. Lett.* **2003**, *91*, 146401.

[34] T. Yanai, D. P. Tew, N. C. Handy, *Chem. Phys. Lett.* **2004**, *393*, 51.

[35] J. Tomasi, B. Mennucci, R. Cammi, *Chem. Rev.* **2005**, *105*, 2999.

[36] A. K. Rappé, C. J. Casewit, K. S. Colwell, W. A. Goddard, I. I. I. W. M. Skiff, *J. Am. Chem. Soc*. **1992**, 114, 10024.

[37] C. -S. Zuo, O. Wiest, Y.-D. Wu, *J. Phys. Chem. A* **2009**, *113*, 12028.

[38] C. Loerbroks, R. Rinaldi, W. Thiel, *Chem. Eur. J.* **2013**, *19*, 16282.

[39] A. Schäfer, C. Huber, R. Ahlrichs, *J. Chem. Phys.* **1994**, *100*, 5829.

[40] A. Schäfer, H. Horn, R. Ahlrichs, *J. Chem. Phys.* **1992**, *97*, 2571.

[41] J. S. Binkley, J. A. Pople, *J. Chem. Phys.* **1977**, *66*, 879.

[42] R. Krishnan, J. S. Binkley, R. Seeger, J. A. Pople, *J. Chem. Phys.* **1980**, *72*, 650.

[43] P. C. Hariharan, J. A. Pople, *Theor. Chim. Acta*. **1973**, *28*, 213.

[44] J. D. Dill, J. A. Pople, *J. Chem. Phys.* **1975**, *62*, 2921.

[45] W. J. Hehre, K. Ditchfield, J. A. Pople, *J. Chem. Phys.* **1972**, *56*, 2257.

[46] M. J. Frisch, J. A. Pople, J. S. Binkley, *J. Chem. Phys.* **1984**, *80*, 3265.

[47] T. H. Dunning, Jr., *J. Chem. Phys.* **1989**, *90*, 1007.

[48] M. J. Frisch, G. W. Trucks, H. B. Schlegel, G. E. Scuseria, M. A. Robb, J. R. Cheeseman, G. Scalmani, V. Barone, B. Mennucci, G. A. Petersson, *et al.*, *Gaussian 09, Revision D.01*., Gaussian, Inc., Wallingford, CT **2009**.

[49] E. F. Pettersen, T. D. Goddard, C. C. Huang, G. S. Couch, D. M. Greenblatt, E. C. Meng, T. E. Ferrin, *J. Comput. Chem.* **2004**, *25*, 1605.

[50] C. C. Pye, *Int. J. Quantum Chem.* **2000**, *76*, 62.

[51] W. Rudolph, M. H. Brooker, C. C. Pye, *J. Phys. Chem.* **1995**, *99*, 3793.

[52] C. C. Pye, M. R. Tomney, T. G. Enright, *J. Anal. Sci. Spectrosc.* **2005**, *50*, 254.

[53] W. W. Rudolph, D. Fischer, G. Irmer, C. C. Pye, *Dalton Trans.* **2009**, 6513.

[54] C. C. Pye, *J. Mol. Struct. THEOCHEM* **2009**, *913*, 210.

[55] H. Ohtaki, T. Radnai, *Chem. Rev.* **1993**, *93*, 1157.

[56] S. Varma, S. B. Rempe, *Biophys. Chem.* **2006**, *124*, 192.

[57] T. M. Alam, D. Hart, S. L. B. Rempe, *Phys. Chem. Chem. Phys.* **2011**, *13*, 13629.

[58] P. E. Mason, S. Ansell, G. W. Neilson, S. B. Rempe, *J. Phys. Chem. B* **2015**, *119*, 2003.

[59] W. Starosta, J. Leciejewicz, *Acta Crystallogr.* **2010**, *E66*, m1561.

[60] R. C. Brüggemann, U. Thewalt, Z. *Naturforsch* **1994**, *B49*, 1531.

[61] Y. Hou, M. A. Rodriguez, M. Nyman, *Cryst. Growth Des.* **2012**, *12*, 1422.

[62] N. Fischer, T. M. Klapötke, K. Peters, M. Rusan, J. Stierstorfer, *Z. Anorg. Allg. Chem.* **2011**, *637*, 1693.

[63] V. Yasodha, S. Govindarajan, J. N. Low, C. Glidewell, *Acta Crystallogr.* **2007**, *C63*, m207.

[64] R. Puchta, B. Neumüller, K. Dehnicke, *Z. Anorg. Allg. Chem.* **2011**, *637*, 67.

[65] V. V. Klepov, A. V. Vologzhanina, L. B. Serezhkina, V. N. Serezhkin, *Radiochemistry* **2013**, *55*, 36.

[66] C. Robl, S. Hentschel, G. J. McIntyre, *J. Solid State Chem.* **1992**, *96*, 318.

[67] C. Robl, S. Hentschel, *Z. Naturforsch* **1990**, *B45*, 1499.

[68] P. E. Mason, S. Ansell, G. W. Neilson, J. W. Brady, *J. Phys. Chem. B* **2008**, *112*, 1935.

[69] H. Lee, M. Diaz, C. B. Knobler, M. F. Hawthorne, *Angew. Chem. Int. Ed.* **2000**, *39*, 776.

[70] J. Cirera, P. Alemany, S. Alvarez, *Chem. - Eur. J.* **2004**, *10*, 190.

[71] a) M. Pinsky, D. Avnir, *Inorg. Chem.* **1998**, *37*, 5575; b) D. Casanova, J. Cirera, M. Llunell, P. Alemany, D. Avnir, S. Alvarez, *J. Am. Chem. Soc.* **2004**, *126*, 1755; c) J. Cirera, E. Ruiz, S. Alvarez, *Chem. Eur. J.* **2006**, *12*, 3162.

[72] J. Frahm, H.-H. Füldner, *Ber. Bunsen-Ges.* **1980**, *84*, 173.

[73] J. P. Austin, N. A. Burton, I. H. Hillier, M. Sundararajan, M. A. Vincent, *Phys. Chem. Chem. Phys.* **2009**, *11*, 1143.

[74] K. J. Laidler, M. C. King, *J. Phys. Chem.* **1983**, *87*, 2657.

[75] E. Wigner, *J. Chem. Phys.* **1937**, *5*, 720.

[76] B. J. Lynch, Y. Zhao, D. G. Truhlar, *J. Phys. Chem. A* **2003**, *107*, 1384.

[77] P. S. Salmon, W. S. Howells, R. Mills, *J. Phys. C Solid State Phys.* **1987**, *20*, 5727.

[78] D. Spangberg, R. Rey, J. T. Hynes, K. Hermansson, *J. Phys. Chem. B* **2003**, *107*, 4470.

[i] Supporting information for this article is available online: https://doi.org/10.1002/qua.25191.